Leadership in Sustainable Infrastructure

Leadership en Infrastructures Durables

Vancouver, Canada

May 31 – June 3, 2017/ *Mai 31 – Juin 3, 2017*

DEBRIS ENTRAINMENT DYNAMICS DURING EXTREME FLOODING EVENTS

Stolle, Jacob[1,4], Goseberg, Nils[2], Nistor, Ioan[1], and Petriu, Emil[3]

[1] Department of Civil Engineering, University of Ottawa, Canada

[2] Ludwig-Franzius-Institute for Hydraulic, Estuarine and Coastal Engineering, Leibniz Universität Hannover, Germany

[3] School of Electrical Engineering and Computer Science, University of Ottawa, Canada

[4] jstol065@uottawa.ca

ABSTRACT: Extreme coastal flooding events, such as the 2005 Hurricane Katrina and 2011 Tohoku Tsunami, have led to an increased emphasis placed on the design of resilient infrastructure. While the primary emphasis has focused on hydraulic load, less consideration has been given to debris loads, particularly in the assessment of the risk of debris loads occurring. The following study examines debris motion in a dam-break wave, physically modelling a tsunami-like event, evaluating the influence of debris configuration and hydrodynamic conditions on debris (lateral) spreading. The debris in this study was modelled as scaled-down shipping containers. The study found that deeper, faster flow conditions limited the influence of the bed surface, resulting in less debris spreading. The initial orientation of the debris also influenced the debris spreading, as the debris rotated to reach an equilibrium orientation. A probabilistic analysis showed that the debris spreading was normally distributed around the mean trajectory of the debris. The objective of this study was to provide a framework for debris load assessment for future design considerations.

Keywords: Debris Transport, Natural Disasters, Tsunami, Dam-Break, Flooding, Hydraulic Engineering

1 INTRODUCTION

With rising sea levels and the prevalence of extreme weather events, increased flooding and extreme hydrodynamic events have been observed worldwide (IPCC 2014). As a result, areas that had previously been not considered a high-risk for flooding have become vulnerable. Meanwhile, the demand for these high-risk areas for tourism, economic, or residential uses has continued unabated (Cooper 2013), therefore regulatory and government agencies have needed to adapt to protect these areas while balancing the other societal needs. One of the primary considerations when assessing the protective needs of a community is to determine the vulnerability of these communities to the increased loads associated with the flooding events.

To this point, the focus of research has been on evaluating the risk of hydraulic loads through flood hazard mapping or tsunami inundation maps (Sorensen 2000). A recent example of developing highly detailed tsunami hazard maps and evacuation modeling for the Indonesian city of Padang was presented by Taubenböck et al. (2013) and (2009). While the hydraulic loads are certainly among the most prevalent loads, loads from debris have been observed in many different flooding events. Several examples of river flooding in Switzerland have shown debris accumulation on structures, such as bridges, resulting in the failure of certain bridges (Schmocker and Hager 2013). Saatcioglu et al. (2005) noted the failure of several structures as a result of debris impact during the 2004 Indian Ocean Tsunami. Robertson et al. (2007) found examples of damaged building piles and columns as a result of debris impact and accumulation during a field survey of the 2005 Hurricane Katrina.

Debris loads are generally addressed as two different loads: a dynamic load associated with debris impact (F_{di}) and a static load associated with debris accumulation (F_{da}). Aghl et al. (2015) developed an equation for maximum debris impact using the conservation of energy principle:

[1] $F_{di} = u\sqrt{m_d k}$

where u is the impact velocity of the debris (m/s), m_d is the mass of the debris (kg), and k is the contact-stiffness between the debris and the structure (N/m). Equation 1 has been used in building standards in the United States for the design of buildings for flooding and tsunami loads (FEMA 2012, Chock 2016). Debris accumulation has been an overlooked topic in relation to flooding events, however highway design standards have often addressed this issue as a result of debris accumulation at bridge piers. In the Canadian Highway Bridge Design Code (2006), the debris accumulation loads are calculated by adjusting the drag coefficient to represent a square pier ($C_D = 1.4$).

To this point, debris loads are designed for throughout a hazard area (FEMA 2012, ASCE 2016). However, in extreme flooding events, large debris, such as vehicles, shipping containers, and shipping vessels, can be entrained within the inundating flow (Robertson et al. 2007, Naito et al. 2014). Designing for these loads throughout a flood hazard area would be expensive and oftentimes unnecessary.

As larger debris tend to have clear source areas (ports, shipping yards, parking lots, etc.) assessing the area at risk for debris impact is viable with an understanding of debris spreading dynamics in extreme flooding conditions. Debris studies in steady-state conditions have often mentioned that debris tended to propagate within the deepest, fastest section (thalweg) of the flow (Bocchiola et al. 2006, Matsutomi 2009, Schmocker and Hager 2013). Naito et al. (2014) presented a method of assessing at-risk areas for debris impact based on a field study from the 2011 Tohoku Tsunami. By determining the source of shipping vessels and surveying the final position, Naito et al. (2014) proposed a ±22.5° envelope from the debris source in the inundation direction. The envelope contained all the shipping vessels identified by the limited field survey.

Nistor et al. (2016) assessed the proposed method by Naito et al. (2014) over flat, horizontal surface with scaled-down shipping containers. Nistor et al. (2016) found that the ±22.5° spreading envelope was a conservative estimation of debris spreading and the spreading angle (θ) was dependent on the number of debris (*N*) present at the debris source.

[2] $\mp\theta = \mp 3.69 \mp 0.80N$

Goseberg et al. (2016b), using the same scaled-down shipping containers, evaluating cases where obstacles (scaled-down buildings) were placed on the flat, horizontal surface. The study found that the obstacles had limited influence on the spreading area as the debris tended to propagate within the deeper, faster sections between the obstacles, resulting in little interaction between the debris and obstacles.

Building guidelines have tended to go with a more conservative estimation of debris motion and have continued to always consider potential debris impacts, however this could be an expensive approach when applied at a wider scale. With the eventual goal to provide an engineering tool to assess the risk associated with large debris impacts during an extreme flooding event, the objectives of this paper are:

- Examine the effect of the hydrodynamic boundary condition on debris spreading.
- Examine the influence of the initial debris configuration on debris spreading.
- Compare the debris spreading to current techniques for analyzing debris spreading.

The study presented here focuses on one type of hydrodynamic boundary condition (a dam-break wave) and examines the influence of the hydrodynamic boundary condition by changing the impoundment depth in the reservoir. The study also only examines one type of debris (shipping containers). The experimental facilities and the experimental protocol are further discussed in Section 2. The results of the experiment are described in Section 3. The results of the experiments are placed within context of the wider literature and scale effect are discussed in Section 4 and 5.

2 EXPERIMENTAL SETUP

2.1 Experimental Facility

The experiments were performed at the Water Resources Laboratory in the Department of Civil Engineering, University of Ottawa, Canada. The experiments were performed in a dam-break flume (DBF), 30 m long, 1.5 m wide, and 0.70 m deep (Figure 1). The reservoir was 21.55 m long and the water was impounded behind a swinging gate, placed on a 0.20 m false floor. The false floor was covered with a fixed layer of 0.001 m sand grains, which resulted in an experimentally-determined Darcy-Weisbach friction factor (f) of 0.014. The swinging gate was manually opened to generate a dam-break wave; a counter weight was placed on the top of the gate to aid in the opening of the gate.

The spatial origin of the experiment (0,0) was considered to be the center of the flume at the upstream edge of the swinging gate. The y-axis was chosen positive in the flow direction, using a right-hand coordinate system, the positive x-direction was to the right and the positive z-direction was up.

The debris was placed on the false floor with the centroid of furthest downstream debris placed center-flume (x = 0 m) at y = 3.20 m. The structure was placed 7.03 m downstream from the gate and was used to measure impact forces for concurrent studies. This aspect of the experiment will not be discussed in the context of this study.

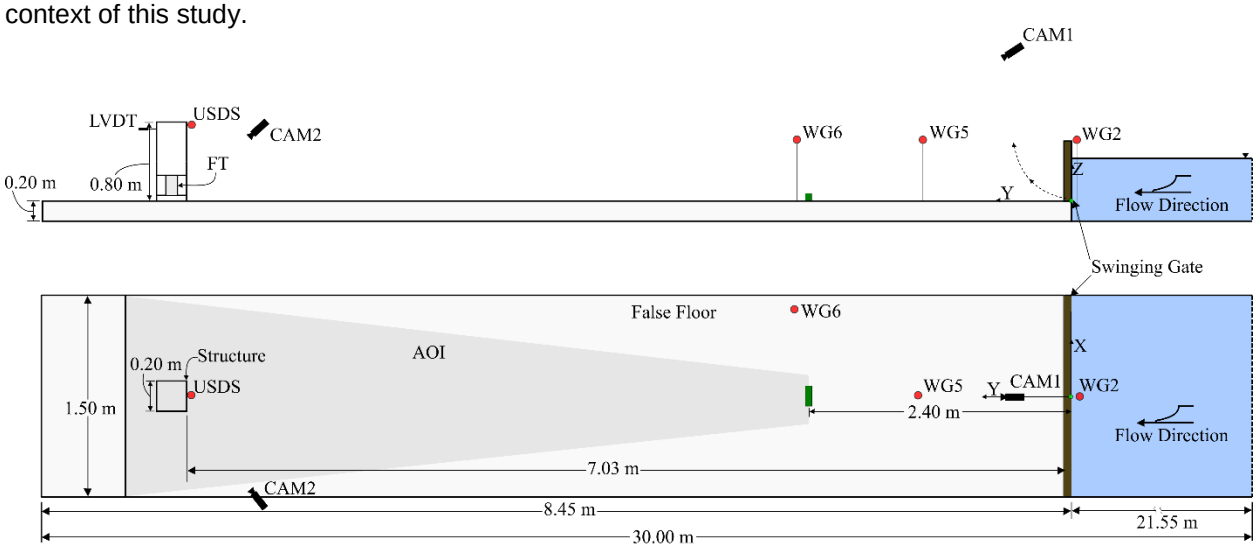

Figure 1. Dam-break Flume (DBF) at the University of Ottawa. The debris source is indicated with a green rectangle. The wave gauge (WG) positions are indicated with a red circle.

2.2 Instrumentation

The time-histories of the water depth were measured using capacitance-type wave gauges (WG) (Akamina Technologies WG-50) with a sampling rate of 1200 Hz. Before installation of the WG, the WG were calibrated with a calibration coefficient greater than 0.99 for each probe. WG2 was placed within the reservoir at y = -0.01 m. The reference time for each experiment was determined as the time that the water depth at WG2 began to decrease, signaling the opening of the gate. An ultra-sonic wave gauge (USDS) (MassaSonic M-5000) was placed at the front face of the structure at a distance of 0.80 m from the false floor.

Two HD cameras (CAM) (Basler AG pi1900-32 gc) were located to analyze the debris trajectories, impact conditions, and bore front profile. The CAM were externally triggered with a 25 Hz sampling rate using an output block signal from a DAQ (National Instruments USB-6009). The area of interest (AOI) of CAM1 is indicated in Figure 1 as the light grey area. Six reference points were placed within the AOI to geo-reference the images from CAM1 to the flume coordinate system.

2.3 Model Debris

The debris consisted of idealized 20-foot shipping containers (ISO668/688) down-scaled based on Froude scaling at a length scale of 1:40. The down-scaled shipping containers were manufactured from positively buoyant polyethylene (PE-HMW, 920 kg/m^3). Each down-scaled shipping container had overall dimensions of 0.06 x 0.06 x 0.15 m with an approximate draft of 0.025 m. The weight of the container, from three

weightings, was determined to be 0.234 kg. The debris uniformly manufactured with a hollow inner shell. A full description of the model debris can be found in Goseberg et al. (2016a).

2.4 Experimental Protocol

The experiments performed in the DBF at the University of Ottawa examined three different experimental configurations, each configuration was repeated at least 10 times (Table 1). The experiments varied the impoundment depth in the reservoir and the orientation of the long-axis of the debris. The impoundment depth was varied between 0.20 m and 0.40 m. The orientation of the long-axis of the debris was placed perpendicular (0°) and parallel (90°) to the flow direction.

For each experiment, the center of the debris was placed 2.40 m from the inner edge of the dam-break gate. The placement of the debris was facilitated by position markers to ensure repeatability between the experimental repetitions. The debris was sealed with petroleum jelly to prevent water from entering the inner volume of the debris. The reservoir was filled to the impoundment depth and allowed to rest to ensure a repeatable hydrodynamic boundary condition. The dam-break gate was then released to form the dam-break wave. Before the beginning of the following experiment, the water was removed from the surface of the false floor.

Table 1. Experimental Protocol

Experimental Category	Impoundment Depth [m]	Debris Orientation [°]	Experimental ID [#]	Repetitions [#]
E01	0.40	0	254-263, 274-283	20
E02	0.20	0	294-303	10
E03	0.40	90	264-273, 284-293	20

2.5 Debris Tracking

The method for tracking the debris used an automated object tracking algorithm developed by Stolle et al. (2016). The algorithm uses a camera-based color thresholding algorithm to identify the green-colored debris within each image, implemented in MATLAB. Due to overtopping of the debris as the surge initially impacted the debris, a Kalman-filter based tracking algorithm was used to maintain the tracking identifier of the debris even when the debris was obscured by the surge. Previous evaluation of the algorithm was found to track the debris with ±0.03 m accuracy (Stolle et al. 2016).

3 RESULTS

3.1 Hydrodynamics

For the experiments, the hydrodynamic boundary condition was a dam-break wave. Contrary to dam-break waves propagating freely throughout the downstream section, in this case, the bore front interacted with the downstream-mounted vertical structure. Although not addressed herein, the flow-structure interaction did affect upstream water levels for conditions where Froude numbers fell short of unity. Figure 2 shows the normalized water elevation profiles from the four WG present in each of the experiments (WG2, WG5, WG6, and USDS). WG2 was placed within the reservoir as close a possible to the face of the gate. The initial decrease in the water surface elevation was used as the opening time of the gate and considered to be the zero-time instance. WG5 and WG6 were placed at 2.00 m and 3.20 m from the gate, respectively. WG6 was placed at the upstream face of the debris at x = 0.61 m (0.14 m from the flume wall).

As can be observed in Figure 2, the hydrodynamic boundary was repeatable between the various experiments. For the different impoundment depths, the time-averaged standard deviation for WG6 was 0.0055 m and 0.0019 m for the 0.40 and 0.20 m impoundment depths, respectively. As the debris propagated predominantly in the bore front, the two impoundment depths showed similar profiles at that position. However, the further from the gate (WG6), the smaller impoundment depths lagged behind the larger impoundment depths. This was potentially due to viscous effects within the bore, as noted by Lauber and Hager (1998) for impoundment depths less than 0.25 m.

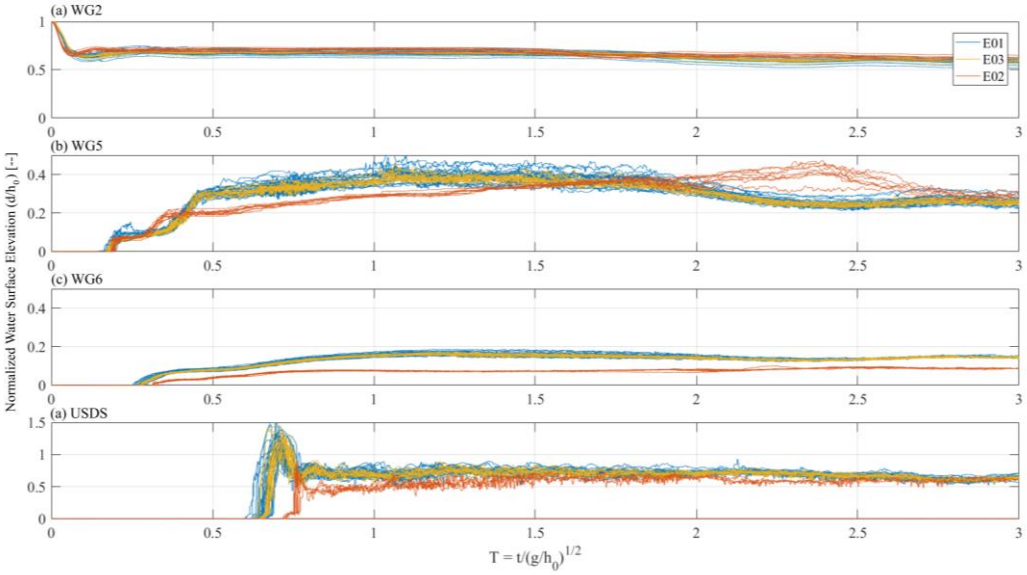

Figure 2. Recorded water surface elevations (D) as a function of time (T) for WG. (a) WG2; (b) WG5; (c) WG6; and (d) USDS.

3.2 Debris Trajectory

Using the debris tracking algorithm discussed in Section 2.5, the trajectory and orientation of the debris were tracked throughout the AOI. As the debris always propagated the length of the flume, the debris spreading (in the lateral direction) was the focus of this study. The mean trajectory of the debris was plotted as a solid line with the 95% confidence interval in Figure 3. The trajectories were compared to the methods proposed by Naito et al. (2014) and Nistor et al. (2016). In all cases, the trajectory of the debris were contained within the methods proposed by Naito et al. (2014) and Nistor et al. (2016).

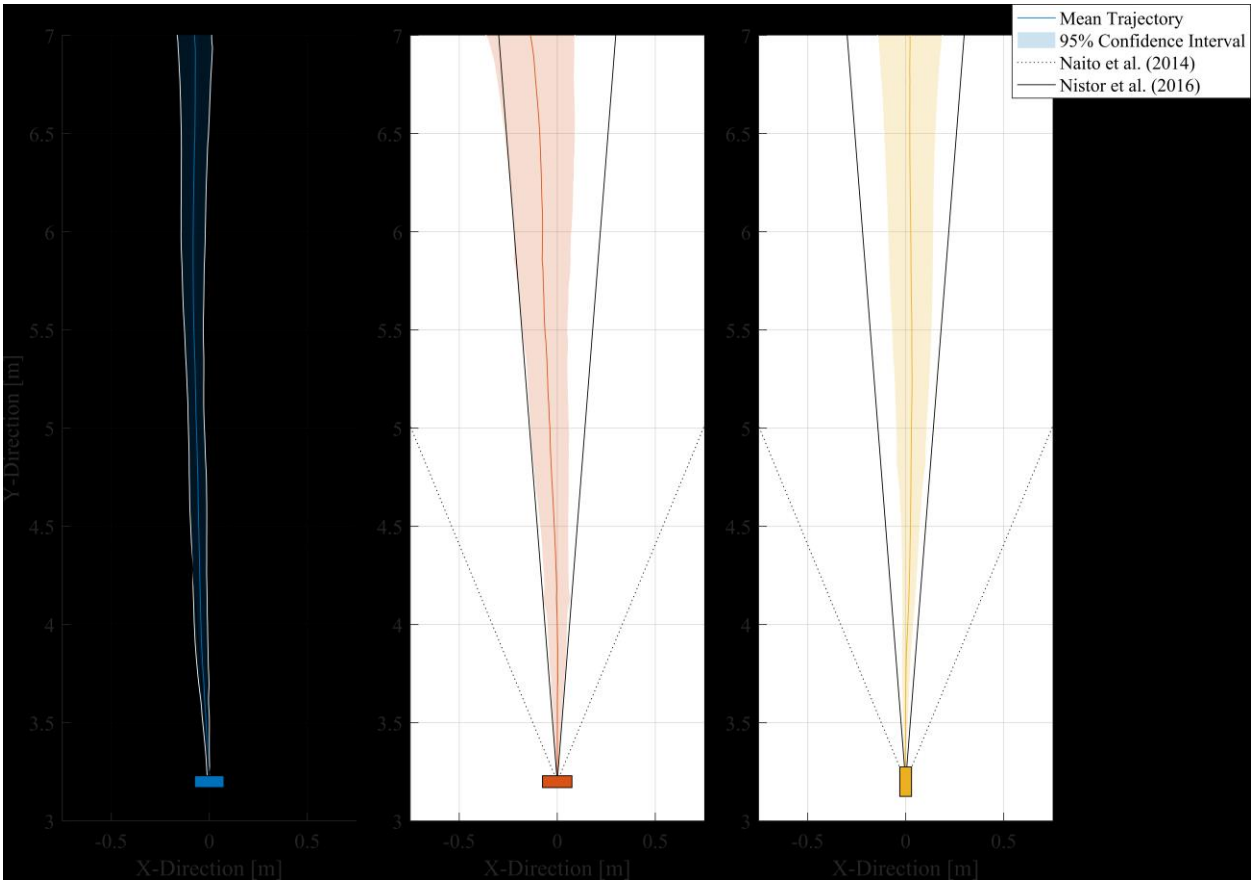

Figure 3. The debris trajectory with the mean trajectory plotted as a solid line, the 95% confidence interval plotted as a faded area. The trajectories are compared to previous literature: Naito et al. (2014) as a dotted line, Nistor et al. (2016) as a solid black line. (a) Impoundment depth of 0.4 m, initial orientation of debris 0^{o}; (b) Impoundment depth of 0.20 m, initial orientation of debris 0^{o}; and (c) Impoundment depth of 0.40 m, initial orientation of debris 90^{o}.

Using an ANOVA test (Freund and Littell 1981), there was significant differences between the three cases (p-value << 0.05). Qualitatively comparing the three cases, less spreading was observed with the larger impoundment depth and the long axis of the debris perpendicular to the flow direction (Figure 3a). The equilibrium propagation orientation of the debris was with the long axis of the debris perpendicular to the flow direction. As a result, there was limited rotation of the debris. In the case with the smaller impoundment depths, the smaller water depths and slower flow velocities resulted in the debris interacting with the bed of the flume. As the debris interacted with the bed, the debris' forward momentum was impeded, forcing the debris to rotate around the point of the debris-bed contact. Similarly, in the case with the long axis of the debris parallel to the flow, the debris rotated towards an equilibrium orientation. The rotation of the debris resulted in increased lateral movement of the debris. Due to the relatively small number of cases examined in this paper, a revised estimate of the spreading angle was not provided as both Naito et al. (2014) and Nistor et al. (2016) equations provide a sufficient conservative estimate for the set of cases presented here.

Figure 4 compares the mean velocity profiles and acceleration distances of the debris for each case, normalized using the theoretical bore front velocity (Chanson 2006). The equilibrium debris velocities closely matched the theoretical flow velocity of a dam-break wave ($\sqrt{gh_0}$ or one-half of the theoretical bore front velocity). In the initial stages of the debris motion, significant overtopping occurred obscuring the debris. Therefore, resulting in larger error associated with the initial stages of debris motion.

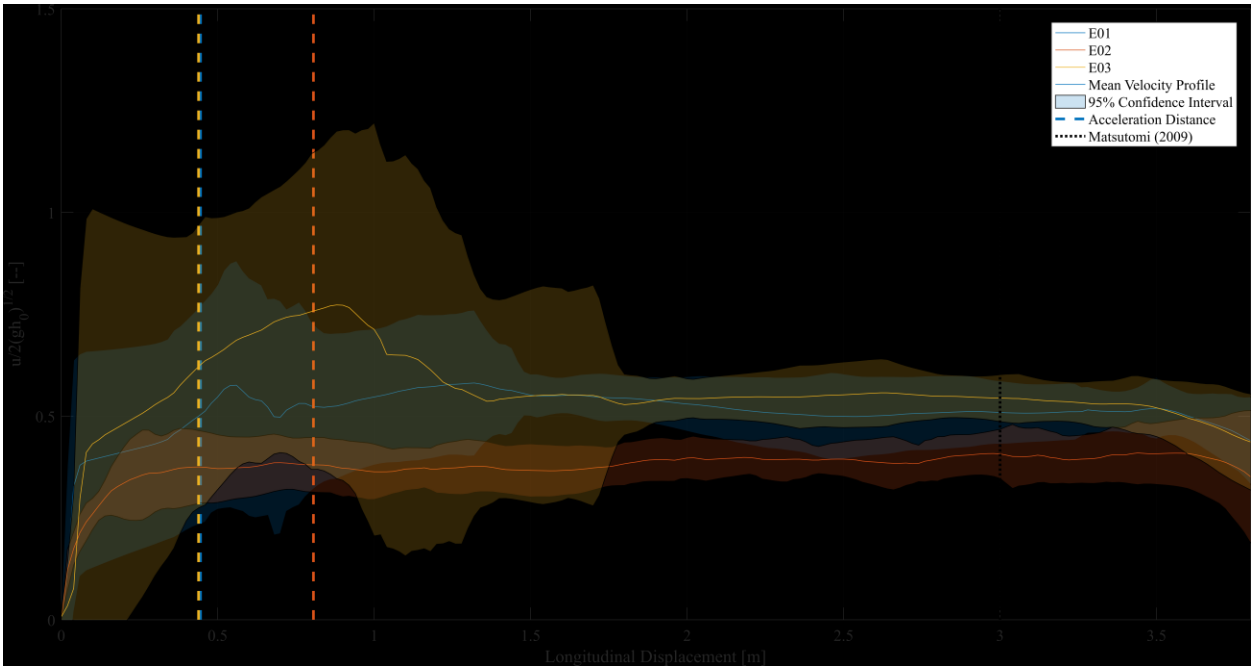

Figure 4. Debris velocity (u) as the debris propagated through the AOI. The solid line represents the mean velocity of the case, the shaded area indicates the 95% confidence interval. The dashed lines show the acceleration distance compared to Matsutomi (2009) (black dotted line).

A comparison between the velocity profiles show an insignificant difference in the acceleration distance and equilibrium velocities of the two cases with 0.40 m impoundment depth (E01 and E03) (Two-sample t-test, p-value >> 0.05). As the debris rapidly rotated to have the long axis perpendicular to the flow direction, the driving (drag) force was similar between the two cases. For the case with the 0.20 m impoundment depth, the acceleration distance and equilibrium velocity were significantly lower. As was discussed in Section 3.1, viscous effect may have resulted in the slower velocities. The acceleration distances for the dam-break case in this experiment were significantly less than the steady-state acceleration distances found by Matsutomi (2009), 20 times the length of the debris (black dotted line).

3.3 Probabilistic Analysis of Debris Trajectory

Both the methods for assessing debris spreading in Section 1 assigns the same risk to all structures within the spreading area. In a similar problem, the Eurocode 1 – Action on Structures (EU 2006) addressed accidental impacts, where an object has a typical trajectory (e.g. car travelling along a road, a ship passing under a bridge), and assessing the risk of the object impacting critical structure members with a Gaussian probability function. Based on the three cases presented, a Shapiro-Wilk test (Shapiro and Wilk 1965) was performed to determine that the spreading was normally distributed. The results of the test around the central y-axis found that the spreading was normally distributed (p-value >> 0.05). In this experiment, the mean of the spreading had a slight bias in the negative x-direction, likely due to inconsistencies in the bed profile of the flume. Figure 5 presents the normal probability density functions of the debris spreading, assuming that the debris was not biased by the bed profile.

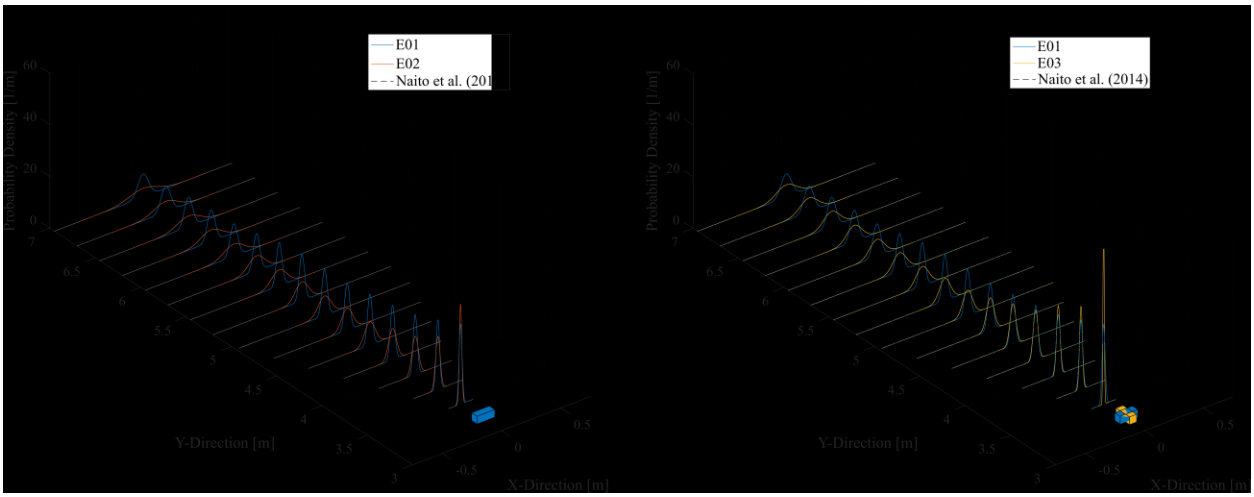

Figure 5. The probability density function for the propagation paths of the debris. (a) compares cases E01 and E02; (b) compares cases E02 and E03.

4 DISCUSSION

The use of dam-break waves has become common to tsunami engineering for the physical modelling of a tsunami wave, particularly in the analysis of loading conditions on structures (Nouri et al. 2010, Al-Faesly et al. 2012). Chanson (2006) revealed, using examples from the 2004 Indian Ocean Tsunami, that a dam-break wave well represented the bore profile of an inundating tsunami wave on a flat coastal plain. Additionally, the dam-break wave can have significantly longer flow duration, and therefore can be more representative of a tsunami wave, compared to a solitary wave, which historically been used for near-shore tsunami wave impingements (Madsen et al. 2008). A dam-break wave is limited by the length of the reservoir, as the negative wave formed at the release of the gate propagates through the reservoir, reflects off the back wall, then interferes with the wave profile in the AOI. As the debris generally propagated through the AOI in less than 5 s, the negative wave, which reached the AOI in > 20 s (Lauber and Hager 1998) should have had no impact on the presented results.

One aspect of the dam-break wave that potentially influences the presented results was the viscous effects in the bore front. A comprehensive dam-break experiment, performed by Lauber and Hager (1998), noted that at impoundment depths of less than 0.25 m, a comparison of the normalized water surface elevation profiles showed significant deviations. Lauber and Hager (1998) indicated that the deviations were likely caused by the viscous forces in the bore front. However, the study presented by Lauber and Hager (1998) focused on the bore front profiles at one normalized distance from the dam-break gate. Further research is needed to understand the influence of the viscous forces in the near- and far-field conditions. As the viscous forces pertain to this study, the reduction in flow velocity could result in the decreased normalized flow velocity observed in Figure 4. The debris velocity was expected to be around the celerity of the disturbance caused by the dam opening ($\sqrt{gh_0}$), which was observed for the 0.40 m impoundment depth. The lower flow velocity for 0.20 m impoundment depth indicate that there are potential viscous effects influencing the flow propagation.

The analysis of debris spreading showed that the spreading of the debris in an ideal flat bottom could be approximated using a normal distribution function, with the spreading angle increasing with distance from the debris source. The determination of the change in spreading angle should be performed at a larger scale to eliminate the potential scale effects related to viscous and friction forces. Further research is required and facilities to conduct those tests need to become available where larger scales could be realized. The combination of the probability density function for debris spreading and the debris acceleration profiles would allow for the development of risk assessment maps for large-scale debris impacts (Figure 6). The risk assessment maps could reduce the cost of designing debris impact resistant structures, as fewer structures would need to be designed for such extreme loads. Figure 6 combines the probability density functions with the mean velocity profile of case E01 by multiplying the force (calculated using Eq. [1]) by the probability density function. In this case, risk is considered to be the probability of a large impact force occurring at a given position.

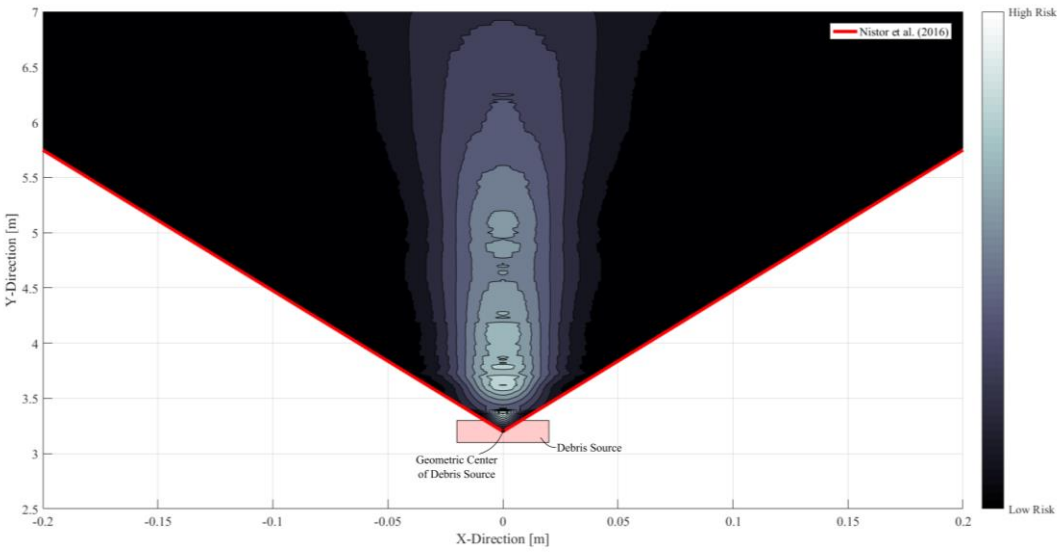

Figure 6. Risk analysis plot for debris loads in extreme flooding events. E01 was used as an example case for these experiments. The risk analysis was constrained by the maximum spreading angle determined by Nistor et al. (2016).

As was observed in Figure 3, as the bed surface was not perfectly flat, the inconsistencies in the bed profile influenced the mean trajectory of the debris. In ideal conditions, the mean trajectory of the debris would be expected to be straight. As the bed profile did have a significant effect, the consideration to the mean trajectory used in determining the central point of the probability density function would be needed. Detailed studies analyzing the influence of bed profile and the influence of built environments should be used to better evaluate the mean trajectory of the debris.

5 CONCLUSIONS

The study presented here analyzes the physical modelling of debris spreading during coastal flooding events, such as storms surges and tsunamis. The experiments were performed at the dam-break facility at the University of Ottawa. The debris was considered as uniform scaled-down shipping container (1:40 length scale), and the motion of the debris was tracked using a camera-based optical tracking algorithm (Stolle et al. 2016). Based on the results, presented in Section 3, the authors concluded:

- Debris spreading increased as a result of the rotation of the debris towards the equilibrium propagation orientation of the debris.
- Deeper, faster flow conditions resulted in less debris spreading due to less interaction with the bed surface.
- The debris spreading area was well within the methods proposed by Naito et al. (2014) and Nistor et al. (2016).
- The spreading of the debris can be considered to be normally distributed around the mean trajectory of the debris.

Debris motion studies, such as the experiment presented here, can be used for better assessment of the risk of large-scale debris impact. Additionally, the work could also be applied to the recovery of valuable equipment and objects in the aftermath of coastal flooding events to aid in narrowing the scope of search operations. However, as discussed in Section 4, there are scale effects related to the relatively small scale of such debris studies. Therefore, further work at larger scales will be needed to address scale effects for these results to be used in real-world applications.

6 ACKNOWLEDGEMENTS

J. Stolle would like to acknowledge the NSERC Canadian Graduate Scholarship (CGS-D) for supporting ongoing research projects at the University of Ottawa. N. Goseberg acknowledges that this research was

supported by a Marie Curie International Outgoing Fellowship within the 7th European Community Framework Programme.

7 REFERENCES

Aghl, P. P., C. Naito, and H. Riggs. 2015. Estimation of demands resulting from inelastic axial impact of steel debris. Engineering Structures 82:11–21.

ASCE. 2016. Minimum design loads for buildings and other structures. . American Society of Civil Engineers.

Association, C. S., and others. 2006. Canadian highway bridge design code. . Canadian Standards Association.

Bocchiola, D., M. Rulli, and R. Rosso. 2006. Transport of large woody debris in the presence of obstacles. Geomorphology 76:166–178.

Chanson, H. 2006. Tsunami surges on dry coastal plains: Application of dam break wave equations. Coastal Engineering Journal 48:355–370.

Chock, G. Y. 2016. Design for tsunami loads and effects in the ASCE 7-16 standard. Journal of Structural Engineering:04016093.

Cooper, N. J. 2013. Innovative Coastal Zone Management: Sustainable Engineering for a Dynamic Coast. Pages 146–147 Proceedings of the Institution of Civil Engineers-Maritime Engineering. . Thomas Telford Ltd.

EU. 2006. Eurocode 1: Actions on structures—.

Al-Faesly, T., D. Palermo, I. Nistor, and A. Cornett. 2012. Experimental modeling of extreme hydrodynamic forces on structural models. International Journal of Protective Structures 3:477–506.

FEMA. 2012. P646 Guidelines for Design of Structure for Vertical Evacuation from Tsunamis. Federal Emergency Management Agency.

Freund, R. J., and R. C. Littell. 1981. SAS for linear models: a guide to the ANOVA and GLM procedures. . Sas Institute.

Goseberg, N., I. Nistor, T. Mikami, T. Shibayama, and J. Stolle. 2016a. Nonintrusive Spatiotemporal Smart Debris Tracking in Turbulent Flows with Application to Debris-Laden Tsunami Inundation. Journal of Hydraulic Engineering:04016058.

Goseberg, N., J. Stolle, I. Nistor, and T. Shibayama. 2016b. Experimental analysis of debris motion due the obstruction from fixed obstacles in tsunami-like flow conditions. Coastal Engineering 118:35–49.

IPCC. 2014. Climate Change 2014–Impacts, Adaptation and Vulnerability: Regional Aspects. . Cambridge University Press.

Lauber, G., and W. H. Hager. 1998. Experiments to dambreak wave: Horizontal channel. Journal of Hydraulic research 36:291–307.

Madsen, P. A., D. R. Fuhrman, and H. A. Schaffer. 2008. On the solitary wave paradigm for tsunamis. Journal of Geophysical Research: Oceans 113.

Matsutomi, H. 2009. Method for estimating collision force of driftwood accompanying tsunami inundation flow. Journal of Disaster Research 4:435–440.

Naito, C., C. Cercone, H. R. Riggs, and D. Cox. 2014. Procedure for site assessment of the potential for tsunami debris impact. Journal of Waterway, Port, Coastal and Ocean Engineering 140:223–232.

Nistor, I., N. Goseberg, T. Mikami, T. Shibayama, J. Stolle, R. Nakamura, and S. Matsuba. 2016. Hydraulic Experiments on Debris Dynamics over a Horizontal Plane. Journal of Waterway, Port, Coastal and Ocean Engineering:04016022.

Nouri, Y., I. Nistor, D. Palermo, and A. Cornett. 2010. Experimental investigation of tsunami impact on free standing structures. Coastal Engineering Journal 52:43–70.

Robertson, I., H. R. Riggs, S. C. Yim, and Y. L. Young. 2007. Lessons from Hurricane Katrina storm surge on bridges and buildings. Journal of Waterway, Port, Coastal, and Ocean Engineering 133:463–483.

Saatcioglu, M., A. Ghobarah, and I. Nistor. 2005. Effects of the December 26, 2004 Sumatra earthquake and tsunami on physical infrastructure. ISET Journal of earthquake technology 42:79–94.

Schmocker, L., and W. H. Hager. 2013. Scale modeling of wooden debris accumulation at a debris rack. Journal of Hydraulic Engineering 139:827–836.

Shapiro, S. S., and M. B. Wilk. 1965. An analysis of variance test for normality (complete samples). Biometrika 52:591–611.

Sorensen, J. H. 2000. Hazard warning systems: Review of 20 years of progress. Natural Hazards Review 1:119–125.

Stolle, J., I. Nistor, and N. Goseberg. 2016. Optical Tracking of Floating Shipping Containers in a High-Velocity Flow. Coastal Engineering Journal:1650005.

Taubenböck, H., N. Goseberg, G. Lämmel, N. Setiadi, T. Schlurmann, K. Nagel, F. Siegert, J. Birkmann, K.-P. Traub, S. Dech, and others. 2013. Risk reduction at the Last-Mile: an attempt to turn science into action by the example of Padang, Indonesia. Natural hazards 65:915–945.

Taubenböck, H., N. Goseberg, N. Setiadi, G. Lämmel, F. Moder, M. Oczipka, H. Klüpfel, R. Wahl, T. Schlurmann, G. Strunz, and others. 2009. Last-Mile" preparation for a potential disaster–Interdisciplinary approach towards tsunami early warning and an evacuation information system for the coastal city of Padang, Indonesia. Natural Hazards and Earth System Science 9:1509–1528.